Available online at www.sciencedirect.com
ScienceDirect
Deep-Sea Research II 55 (2008) 752–765
DEEP-SEA RESEARCH PART II
www.elsevier.com/locate/dsr2

Virioplankton dynamics and virally induced phytoplankton lysis versus microzooplankton grazing southeast of the Kerguelen (Southern Ocean)

C.P.D. Brussaard[a,*], K.R. Timmermans[a], J. Uitz[b], M.J.W. Veldhuis[a]

[a]*Royal Netherlands Institute for Sea Research, P.O. Box 59, 1790 AB Den Burg, The Netherlands*
[b]*Laboratoire d'Océanographie de Villefranche, CNRS UMR 7093 and Université Pierre et Marie Curie, Quai de la Darse B.P. 8, 06 238 Villefranche-sur-Mer Cedex, France*

Accepted 9 December 2007

Abstract

Viral dynamics, community structure, and the impact of viruses on phytoplankton mortality in comparison with microzooplankton grazing were determined in the natural iron-fertilized waters southeast of the Kerguelen Islands, Southern Ocean, during the austral summer (January–February 2005). The study area was characterized by a phytoplankton bloom above the Kerguelen Plateau and the high-nutrient low-chlorophyll waters surrounding it. During the Kerguelen Ocean and Plateau compared Study (KEOPS), viral abundance was relatively high ($1–19 \times 10^7\,mL^{-1}$) as compared to the few other studies in the Southern Ocean, significantly correlating with depth and system productivity. Viral abundance showed a strong positive relationship with the numerically dominant bacterial hosts, which in turn were correlated to phytoplankton biomass. In total, 13 different viral genome sizes were detected, with the lower-sized genomes 34 and 68 kb dominating at all stations. The viral community at the low chlorophyll C-transect grouped apart from the more productive transects A and B. Potential algal viruses were recorded for all stations, but only at very low intensities. Virally induced lysis of the smaller-sized ($<10\,\mu m$) phytoplankton was a minor loss factor as compared to microzooplankton grazing (up to 6% and 45% of total $<30\,\mu m$ algal standing stock per day, respectively). Grazing was phytoplankton population-specific, but was in all cases able to keep the standing stock of the small-sized phytoplankton low (net growth rates between -0.2 and $0.2\,d^{-1}$). Microzooplankton regenerated on average $1.1\,pM\,Fe\,d^{-1}$ (present study), which represented approximately 30% of the total regeneration rate and at least 15% of the total biogenic Fe demand as calculated by [Sarthou, G., Vincent, D., Christaki, U., Obernosterer, I., Timmermans, K.R., Brussaard, C.P.D., 2008. The fate of biogenic iron during a phytoplankton bloom induced by natural fertilization: impact of copepod grazing. Deep-Sea Research II].

Keywords: Bacteria; Distribution; Grazing; Lysis; Phytoplankton; Viruses; Southern Ocean; Kerguelen Plateau; 48–52°S and 72–78°E

1. Introduction

Viruses are ubiquitous and abundant components of the marine environments, generally found at abundances of 10^5–$10^8\,mL^{-1}$ (Suttle, 2005; present study). Field studies and laboratory experiments indicate that viruses are of ecological importance, directly affecting population dynamics, community structure, diversity, and genetic transfer (Wommack and Colwell, 2000; Weinbauer, 2004). Viruses act as catalysts as they play a key role in transforming host cells into more bio-available dissolved organic matter (Gobler et al., 1997; Wilhelm and Suttle, 1999). There are now compelling data showing that viruses play an important role in marine biogeochemical cycling (Fuhrman, 1999; Ruardij et al., 2005; Suttle, 2005). Various contrasting marine environments have been investigated to support these conclusions, but only a few studies have directly addressed viral ecology in the open Southern Ocean (Smith et al., 1992; Marchant et al., 2000; Guixa-Boixereu et al., 2002; Strzepek et al., 2005).

The Southern Ocean is the largest oceanic area and occupies the only band of latitudes on Earth where ocean

*Corresponding author. Tel.: +31 222 369300; fax: +31 222 319674.
E-mail address: corina.brussaard@nioz.nl (C.P.D. Brussaard).

0967-0645/$ - see front matter © 2008 Elsevier Ltd. All rights reserved.
doi:10.1016/j.dsr2.2007.12.034

waters circle the globe. Its unique geography has profound implications for the global ocean circulation and the Earth's climate system. This ocean region is also a major high-nutrient low-chlorophyll (HNLC) system, where algal biomass remains low despite the high concentrations of the inorganic major nutrients. Very low iron (Fe) concentrations, combined with the absence of sources of Fe, is considered as the main factor controlling phytoplankton production in these regions (Blain et al., 2001; De Baar et al., 2005). Furthermore, the depth of the wind-mixed layer, in regulating the light climate, is an important factor controlling photosynthesis in HNLC regions (reviewed in De Baar et al. (2005)). To support total primary production, input of new Fe (Blain et al., 2007) but also recycling of Fe are thought to play an important role (Kirchman, 1996; Strzepek et al., 2005). Most of the total dissolved Fe in seawater is complexed by dissolved organic ligands, and constitutes, as such, the largest potential pool of bioavailable Fe to marine plankton (Rue and Bruland, 1997). Besides the ability of zooplankton to regenerate Fe from prey (Hutchins and Bruland, 1994; Landry et al., 1997; Smetacek et al., 2005), virally induced lysis may play a critical role in the recycling of organically complexed Fe (Gobler et al., 1997; Poorvin et al., 2004; Mioni et al., 2005). It has been suggested that the naturally occurring viral populations in HNLC regions could supply a substantial fraction of the daily phytoplankton demand for recycled Fe (Poorvin et al., 2004).

Within the Southern Ocean, there are, however, a few selective regions that show annually recurrent phytoplankton blooms (Blain et al., 2001). One such site is the Kerguelen Plateau, centered around 51°S and 75°E. The KEOPS project (Kerguelen Ocean and Plateau compared Study, 2005–2007) was launched to test the mechanisms and effects of natural iron fertilization of the oceanic HNLC water over the Kerguelen Plateau on the biological CO_2 pump during the austral summer. At the time of the expedition, an algal blooms was observed on the Kerguelen Plateau, visible by satellite images (Blain et al., 2007). Enhanced vertical mixing due to internal waves increased the upward transport of iron (and major nutrients) indispensable to sustain a phytoplankton bloom (Park et al., 2008a), thereby replenishing very efficiently the surface layer with iron. For comparison a deep-water, open-ocean, area was studied as a reference of the typical HNLC regions.

This paper aims to describe (1) the dynamics of viruses in relation to their most abundant hosts (bacteria and phytoplankton) during the austral summer (January–February 2005) over the Kerguelen Plateau (Southern Ocean) at three transects across the plateau, representing the bloom region to the HNLC area. Other objectives were (2) to examine the diversity of the viruses in the surface water layer, (3) to determine the actual virally induced mortality of smaller-sized phytoplankton and compare it to microzooplankton grazing, and (4) to estimate the share of the mortality factors for the biogenic Fe budget.

2. Material and methods

2.1. Study area and sample collection

Samples were collected in the waters southeast of the Kerguelen Islands (Southern Ocean) during the KEOPS expedition from 19 January to 13 February 2005 on board R/V *Marion Dufresne* (Fig. 1). Three transects (10–11 stations each) were sampled at various depths (down to 3500 m). Two main reference stations were visited several times: station A3 (50°38S, 72°05E) was located in the core of a phytoplankton bloom above the Kerguelen Plateau and typical of Fe-enriched waters, whereas station C11 (51°39S, 78°00E) was located outside the bloom area and typical of HNLC conditions (Blain et al., 2007). Water samples were collected with 12-L Niskin bottles mounted on a rosette frame with a Sea Bird SBE-911 plus CTD sensor.

2.2. Microbial community

The abundance of viruses was determined according to Brussaard (2004). In short, glutaraldehyde-fixed samples (final concentration 0.5% glutaraldehyde, flash-frozen in liquid nitrogen and stored at −80 °C prior analysis) were diluted (>50 times) in TE-buffer (pH 8) after thawing, stained with the nucleic acid-specific dye SYBR Green I (final concentration of 0.5×10^{-4} of the commercial stock; Invitrogen) for 10 min in dark at 80 °C, and analyzed using a benchtop Beckton-Dickinson FACSCalibur flow cytometer. Virus counts were corrected for the blank consisting of TE-buffer with sterile 0.2-μm-filtered seawater in the correct dilution. Different virus populations (V1, V2, and V3) were discriminated on the basis of the green fluorescence and side scatter signature (Fig. 2).

Bacterial abundance also was determined on 0.5% (final concentration) glutaraldehyde-fixed samples (flash-frozen and stored until analysis at −80 °C) using a Becton-Dickinson FACSCalibur flow cytometer (Marie et al., 1999). In summary, samples were diluted with TE-buffer

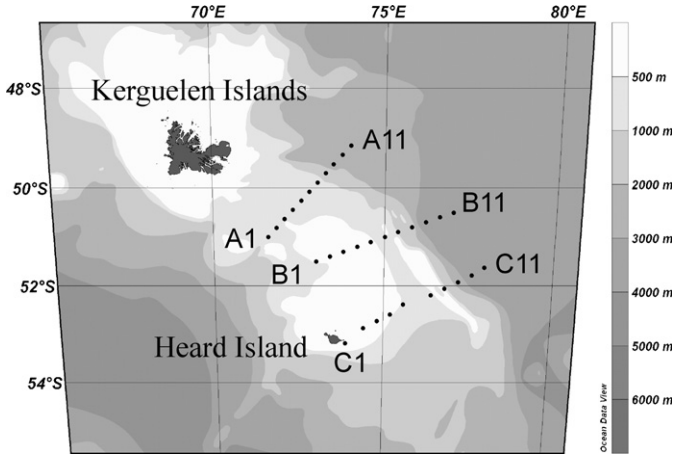

Fig. 1. Area of study and locations for the KEOPS 2005 cruise.

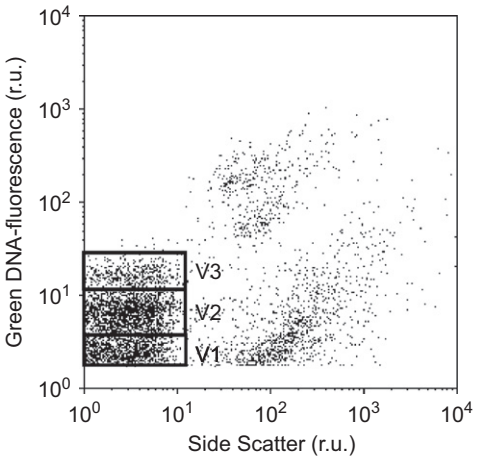

Fig. 2. Flow cytometric cytogram of the typical viral community during KEOPS 2005. The viral community is composed of three viral groups (V1, V2, and V3) discriminated based on the intensity of their green fluorescence after staining with the nucleic acid-specific dye SYBR Green I and the side-scatter signal.

(pH 8) five-fold, stained with SYBR Green I at a final concentration of 1×10^{-4} of the commercial stock for 15 min in dark at room temperature.

Phytoplankton <30-μm diameter was enumerated using a Beckman Coulter XL-MCL flow cytometer. Phytoplankton was discriminated from other particles based on the red fluorescence signal of the autofluorescence of chlorophyll. Different subpopulations were discriminated on the basis of their autofluorescence and relative size (Veldhuis and Timmermans, 2007). The photochemical efficiency of photosystem II (F_v/F_m) of the algal community was measured using a PAM fluorometer (PHYTOPAM, Walz, Germany) according to Timmermans et al. (2008).

For total community chlorophyll a (Chl *a*) analysis, 1.5–2.8 L of sample were filtered through a 25-mm glass-fiber filter (GF/F Whatman), after which the samples were flash-frozen until analysis according to Van Heukelem and Thomas (2001) using an Agilent Technologies 1100 HPLC system.

2.3. Dilution assay

The virally induced mortality and microzooplankton grazing rates of the phytoplankton <20 μm in diameter was estimated at six stations at a depth of 20–40 m according to Baudoux et al. (2006). In short, two dilution series of the 200-μm mesh-size screened natural sample were prepared: one series with 0.2-μm pore-size (Poretics, Millipore) filtered natural sample according to Landry and Hassett (1982), and one series with 30 kDa (polyether sulfone membrane, Vivaflow 200, Vivascience) filtered natural sample. All materials used for the experiments were carefully acid-cleaned, rinsed with MilliQ, and finally with the sample prior to use. Viral lysis rate could be estimated from the difference between the two dilutions series. Dilutions of 20%, 40%, 70%, and 100%, the natural water were prepared in triplicate in 300-mL soft polycarbonate incubation bottles. At the start of the incubation, a 5-mL subsample was taken from each incubation bottle, after which the bottles were squeezed and closed in such a way that no air bubble was trapped in the bottle. All bottles were mounted on a slowly rotating (0.5 rpm) plankton wheel and incubated at in situ temperature (2–4 °C) and irradiance (13–50 μmol quanta $m^{-2} s^{-1}$, light period of 12 h). After 24 h incubation, another 5-mL subsample was taken to monitor phytoplankton growth. The photosynthetic efficiency (F_v/F_m) of the algal community did not alter during the 24-h incubation, indicating that the photosynthetic community did not experience additional iron stress (Behrenfeld and Kolber, 1999). Phytoplankton abundance was determined (in triplicate samples) directly upon sampling using flow cytometry. Four algal populations were differentiated that were numerically abundant enough to allow proper analysis. The estimated cell diameters were on average 1.7, 3.0, 4.7, and 6.3 μm, with average cellular carbon contents of 1.2, 5, 13, and 30 pg C $cell^{-1}$, calculated using the calibration method of Veldhuis and Timmermans (2007). At station B5, the algal abundance at the start of the experiment was so low that the assay was terminated. The generally low abundance of the smaller-sized phytoplankton (maximum abundance 3.5×10^3 mL^{-1}) was also the reason that not all phytoplankton groups were always included in the analysis. The apparent growth rate (μ_{app}, d^{-1}) was calculated for each sample from the changes in abundance during the incubation.

The regression coefficient of apparent growth rate versus dilution factor for the 0.2-μm series provided the microzooplankton grazing rate (M_g, d^{-1}) and for the 30-kDa series provided both the grazing and virally induced mortality rate (M_{g+v}, d^{-1}). The specific virally induced mortality rate (M_v, d^{-1}) was obtained from the difference in M_{g+v} and M_g. The specific growth rate (μ, d^{-1}) could be determined as the *y*-axis intercept value of the regression line obtained with the 30-kDa series. The significance (*p*) of the slope (M_g and M_{g+v}) and the intercept (μ) was determined performing a *t*-test on the regression analysis. The significance (*p*) between the slopes of the regressions lines (i.e., significance of M_v) was also estimated using a *t*-test.

2.4. Virus diversity

From a 20–40 m depth, 10-L samples were preconcentrated for viral diversity analysis by 30-kDa MWCO ultrafiltration (Vivaflow 200), clarified of bacteria and cell debris in the presence of Tween 80 (0.008%, v/v, final concentration) by low-speed centrifugation (10,000*g*, 30 min at 4 °C, fixed angle rotor F-34-6-38, Eppendorf 5810R), and concentrated to a final 1–3 mL by 30 K MWCO PES-membrane Vivaspin concentrators (VivasScience, Sartorius Group). Concentrates were flash-frozen and stored at −80 °C until further analysis in the

home laboratory. After thawing, the supernatant was harvested by ultracentrifugation (141,000*g*, 2 h at 8 °C, fixed angle rotor TFT 55.38 rotor, Centrikon T-1080, Kontron Instruments) and pellets were resuspended in SM buffer. Three plugs of this concentrate were prepared in molten 1.5% (w/v) InCert agarose (Cambrex Bioscience, Rockland, ME USA) and digested overnight at 30 °C in a lysis buffer (250-mM EDTA, 1% SDS (v/v), 1 mg mL^{-1} proteinase K (Sigma-Aldrich). Samples were loaded onto a 1% SeaKem GTG agarose gel (Cambrex Bioscience) in 1 × TBE buffer. The gel was run using a Bio-Rad DR-II CHE pulsed field gel electrophoresis (PFGE) cell unit operating at 6 V cm^{-1} at 14 °C in 0.5 × TBE tank buffer. Two pulse ramp settings were used: 1–6 s for 20 h to discriminate the smaller virus genomes, and 8–30 s for 20 h to check for larger virus genomes. After electrophoresis, gels were stained for 1–3 h with SYBR Green I (1×10^{-4} of commercial solution, Invitrogen), destained for 10 min in MilliQ (Gradient A10, Millipore), and analyzed using a FluorS imager (Bio-Rad Instrument). Sizing of the viral genomes was performed against a 5-kb lambda ladder, a lambda concatamers ladder (both Bio Rad, Richmond, CA), and a quantitative DNA molecular weight marker (Hyperladder VI; Gentaur Molecular Products). The molecular weight and DNA content of each band was determined by image analysis and comparison with the markers, allowing the number of putative genome copies to be calculated. The total number of viruses per sample plug ranged between 1.5 and 9.9×10^8. The relative abundance (%) of the total detected virus genomes present in each band was calculated.

3. Results

3.1. Brief overview of the study area

The physio-chemical features of the study area and the satellite images are discussed in more detail by Blain et al. (2001, 2007) and relevant papers in this issue. Relevant to know for the understanding of the present study is that the Polar Front, responsible for bringing in cold and nutrient-rich water, passes south of the Kerguelen Islands and goes northeastward, skirting the continental slope (Park et al., 2008b). During the austral summer, surface water above the archipelago had a temperature of 2–4 °C. The concentrations of nitrate and inorganic phosphate were high for the entire study area and remained also high during the entire study (>20 and 1.2 μM, respectively), whereas the concentration of silicic acid was high at the C-transect (>10 μM) but relatively low (<2 μM in upper 100 m) at stations 1–5, transect A. The concentration of dissolved iron (DFe) was subnanomolar (about 0.1 nM) in 0–125 m, but increased with depth above the plateau (Blain et al., 2008). A phytoplankton bloom was observed above the Kerguelen Plateau, with the shape of the bloom at the southeastern side constrained by the bathymetry and a plume extending northeast of the island showing a high mesoscale and temporal variability (Blain et al., 2007). The bloom was dominated by diatoms in measure of cellular carbon (Armand et al., 2008). The conditions found over the Plateau were indicative of a large diatom bloom in its last stage of development, limited by the low concentration of dissolved silicic acid (Mosseri et al., 2008).

3.2. Spatial horizontal distributions at 20–40 m depth

The horizontal distribution of viruses at 30-m depth (Fig. 3A) showed the highest abundance of 1–1.5 × 10^7 mL^{-1} above the Kerguelen Plateau in the western part of the study area (transects A and B) and the lowest in the HNLC region (B11 and C11; $<4.5 \times 10^6$ mL^{-1}). The low viral abundance corresponded to the lowest abundance of the numerically dominating bacterial hosts in the HNLC region (Fig. 3B). The ratio of viruses to bacteria (VBR) varied between 9 and 37 and was highest in the Kerguelen bloom area (Fig. 3C). The second numerically important potential host of viruses are the smaller-sized phytoplankton (<20 μm), dominated by <7-μm algae (pico- and nanophytoplankton). Highest abundances were also recorded in the south, up to four-fold higher at stations 1–5 of transect C (Fig. 3D). When expressed in total cellular carbon, however, these small-sized phytoplankton showed their maximum biomass at stations 1–5 of transects A and B (Fig. 3E). Total Chl *a*, including all size classes, showed a similar distribution (Fig. 3F). Total Chl *a* was dominated by diatoms, constituting for at least 95% of the total algal biomass. The algal community had a good photosynthetic efficiency at stations 1–5 of all three transects (F_v/F_m of 0.45–0.6), independent whether the larger or smaller phytoplankton dominated numerically. F_v/F_m decreased towards the true HNLC region in the southeast of the study area, with lowest values (<0.3) at stations B10, B11, and C11.

Using the Spearman test for non-parametric correlation, we found viral and bacterial abundances at 30-m depth only weakly correlated (Spearman rank order correlation coefficient, $r_S = 0.24$, $p = 0.033$; Table 1). The average virus to bacterial host ratio (VBR) was 20 ± 9 (mean ± S.D.; $n = 79$). VBR was strongly correlated to viral abundance ($r_S = 0.92$, $p < 0.0001$) and only weakly to bacterial abundance ($r_S = -0.10$, $p = 0.368$), indicating that the ratio was mainly determined by variations in viral abundance. Indeed, bacterial abundance was overall 3–6 × 10^5 mL^{-1}, whereas the viral abundance varied an order of magnitude between 2.5×10^6 and 6.5×10^7 mL^{-1}. Viral abundance correlated, furthermore, negatively with the smaller-sized phytoplankton abundance, but positively with phytoplankton biomass (Table 1).

Within the viral community, the group V1 dominated and comprised between 60% and 85% of the total virus abundance (Fig. 2). The virus group V2 made up between 13% and 35%, with the lowest contribution at stations C7–C11 of transect C. The contribution of group V3 ranged between 1.5% and 10% with the lowest values for transect A.

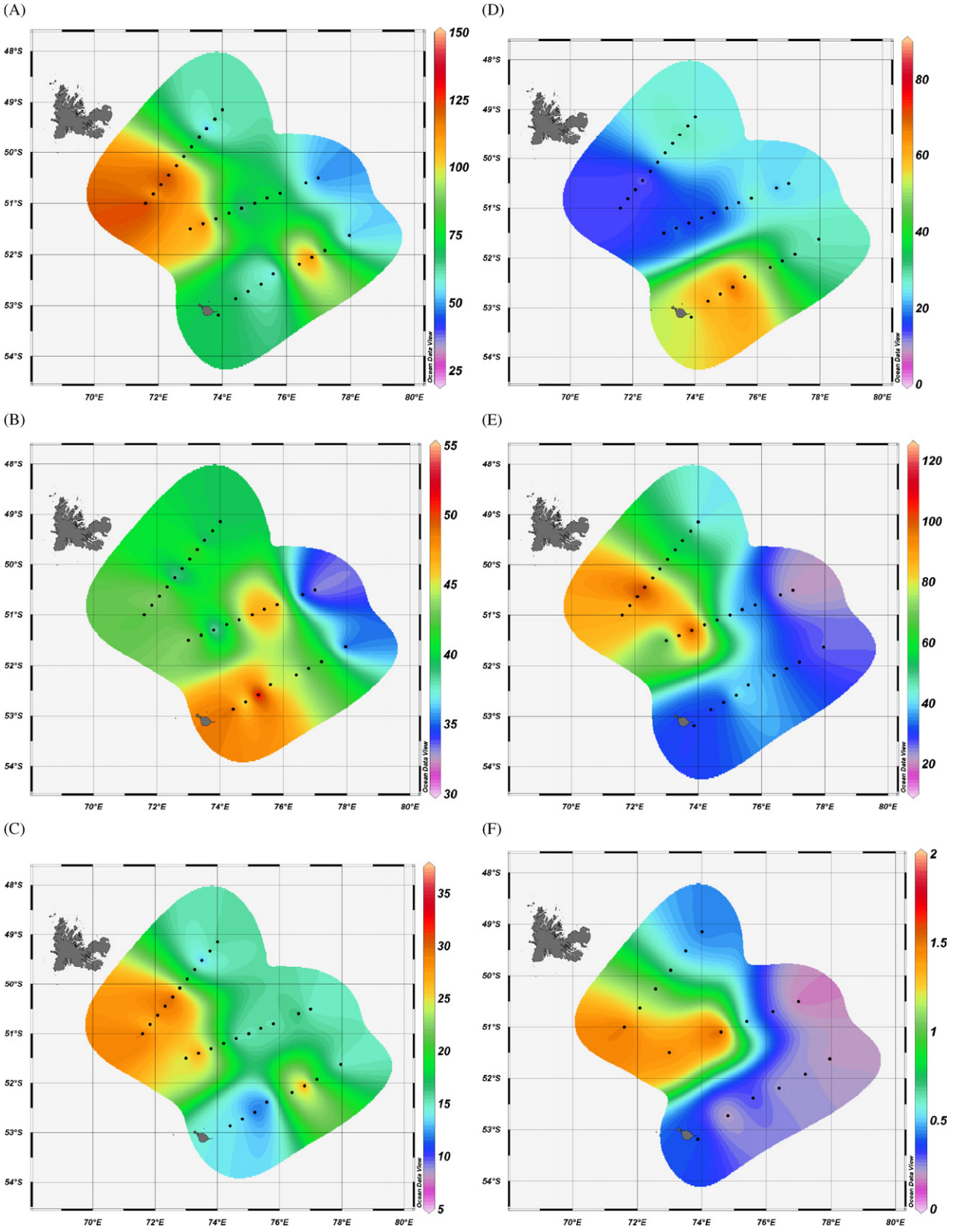

Fig. 3. Spatial horizontal (30-m depth) distributions during the KEOPS 2005 cruise: (A) viral abundance ($\times 10^5$ mL^{-1}), (B) bacterial abundance ($\times 10^4$ mL^{-1}), (C) virus to bacteria ratio (VBR), (D) abundance of phytoplankton <20-μm diameter ($\times 10^2$ mL^{-1}), (E) biomass of phytoplankton <20-μm diameter (μg C L^{-1}), and (F) total Chl *a* (μg L^{-1}).

Table 1
Correlations between the viral abundance (virus), the bacterial abundance (bact), and the abundance (algae) and biomass (algal C) of the phytoplankton with cell diameters <20 μm (enumerated by flow cytometry) at 30 m, using the non-parametric Spearman rank order test

	bact	Chl *a*	algae	algal C
Virus	0.240	0.587	−0.436	0.549
	0.033	0.000	0.000	0.000
	79	42	76	75
Bact		0.283	0.250	0.091
		0.070	0.031	0.439
		42	75	74

Presented in vertical order: the Spearman correlation coefficient (r_S), the *p*-value, and the number of samples.

Table 2
Relative abundance (%) of distinct viral populations, defined by genome size (kb), using PFGE

Station	Viral genome size (kb)						
	30	34	40	54	68	75	80
A1	11	42		15	43		
A3-1	2	45	3	14	36		0.3
A3-2	3	34	1	13	44		5
A3-3	0.2	75	0.1	6	19		0.1
A3-4	8	53		10	24		4
A5	0.2	30		12	47		10
A7	6	21		16	57		
A9	7	28		26	39		
B3	13	28	10	14	35		
B5	10	18	0.2	18	54		
B7	15	24	8	17	37		
C3		4		16	76	5	
C5		9		22	57	12	
C7		19		21	60	0.2	
C9				23	63	14	
C11-1				19	69	12	
C11-2				20	70	11	

Larger genome sizes (see text) have been recorded, but the intensities were too low to allow quantification.

The viral diversity as determined by PFGE displayed up to 13 bands per sample, ranging in genome size from 30 to 226 kb. The band intensities of the viral genomes >80 kb (95, 101, 130, 143, 147, 150, 163, 175, 185, 203, 215, 226 kb) were not high enough to allow proper quantification and, thus, the relative abundance was calculated only for the genome sizes between 30 and 80 kb (Table 2). The most common viral genome sizes were found to be 34 and 68 kb. The latter genome size showed its highest contribution for the C-transect (57–76% of the total virus community). The 75-kb viral genome was even more exclusive being only found at the transect C stations. The other abundant band representing the 54-kb viral genomes was found at all stations and comprised on average 17% of the total virus community. Statistical analysis, using a simple Jaccard correlation test for binary data (presence/absence of PFGE bands) in combination with multidimensional scaling (MDS), showed that the C-transect stations grouped together, and were clearly distinguishable from transects A and B (data not shown). No clear relationship with the location of the stations in the transect was observed. The distribution of the viral community at the main process station C11 was a stable one as the recurrent sampling (C11-1 and C11-2 with 8 days in between the samplings) provided identical results. Although for the other main process station, A3, some differences between four recurrent samplings (approximately 1 week in between samplings) were evident, there was an overall similarity in distribution. Station A3-4 showed the most larger-sized viral genomes (95, 101, 130, 143, 150, 175, 203, and 226 kb), followed by C3 and C5 (147, 150, 185, and 215 kb). Due to the generally low intensities of the bands, it cannot be excluded that these larger viral genomes were also present at the other stations. This poor resolution was partly caused by the low efficiency of sample concentration, directly affecting the intensities of the less abundant viral genomes.

Virally mediated mortality rates and the microzooplankton grazing rates of the smaller-sized phytoplankton at seven stations are presented in Table 3. Virally induced mortality rates were generally not significantly different from zero, although a weak evidence consisted for stations A3-3, C5, and C11. Viral lysis rates at these stations were 0.09, 0.11, and 0.18 d^{-1} for the various subpopulations, representing a daily loss of maximum 6% of the total <30-μm (flowcytometrically detectable) algal standing stock. Microzooplankton grazing was the most important loss factor of pico- and nanophytoplankton, independent of the transect or station (Table 3). Losses up to 40 μg C L^{-1} d^{-1} per algal subpopulation were recorded, representing up to 45% of the total <30-μm algal standing stock. A severe drop in grazing on the 3-μm algal cluster was recorded with time (17-day interval). At the same time, the specific growth rate of this population declined from 0.42 to 0.24 d^{-1}. The growth rates were highly variable for the different phytoplankton groups, and stations and occasionally at the C-stations even negative.

3.3. Spatial vertical distributions

The vertical distribution of viral abundance showed variation with depth for all three transects (Fig. 4), but with always the highest abundances in the surface mixed layer. Overall, viral abundance ranged from 1 to 19×10^6 mL^{-1}. Using the ANOVA analysis of variance, the viral distribution was found to be significantly ($p<0.001$) affected by depth and the distance of the stations to the Kerguelen Plateau (stations were divided into three classes: stations 1–3, 4–7, and 8–11 based on location and depth), but not by the transect ($p=0.395$). Spatial depth variations of the viral subgroups V1–V3 indicated that V1 dominated (>80% of total virus abundance) the deeper waters (>500 m; profile not shown).

Table 3
Viral lysis, microzooplankton grazing and growth rates (d^{-1}) calculated from the dilution assay for the four phytoplankton groups (differing in size)

	Station					
	A3-1	A3-3	A11	B1	C5	C11-1
Viral lysis rates (d^{-1})						
1.7 μm					0.11[a]	0[a]
3.0 μm	0[a]	0[a]	0.04[a]	0[a]	0[a]	0.18[a]
4.7 μm			0[a]			0[b]
6.3 μm		0.09[a]				
Viral lysis ($\mu g\,C\,L^{-1}\,d^{-1}$)	0	2.8 (1)	0.0	0	0.3 (1)	1.9 (6)
Grazing rates (d^{-1})						
1.7 μm					0[a]	0.40[a]
3.0 μm	1.78[d]	0.11[d]	0.10[d]	0.30[d]	0.17[d]	0.15[c]
4.7 μm			0.62[d]			0.21[d]
6.3 μm		0[d]				
Grazing ($\mu g\,C\,L^{-1}\,d^{-1}$)	40 (45)	5.6 (2)	11 (21)	14 (18)	0.3 (1)	4 (14)
Growth rates (d^{-1})						
1.7 μm					−0.01[d]	−0.19[d]
3.0 μm	0.42[d]	0.24[c]	0.06[d]	0.50[d]	0.21[d]	−0.13[c]
4.7 μm			0.38[d]			0.28[c]
6.3 μm		0.28[c]				

Total viral lysis and microzooplankton grazing per station expressed in $\mu g\,C\,L^{-1}\,d^{-1}$ are provided with the percentage of standing stock between brackets. Significance (*t*-test) of the mortality and growth rates are listed in the footnote (indicated by coding listed in superscript).
[a] $p > 0.05$.
[b] $p = 0.01$–0.05.
[c] $p < 0.001$.
[d] $p = 0.001$–0.01.

Viral group V2 had its highest contribution at transect A and the shallower stations of transects B and C (approximately 15–35% of total). The share of subgroup V3 was in general minor (<6%), with lowest percentages in the deeper waters and the highest values mainly concentrated above the Kerguelen Plateau.

Taking into account all depths, viral abundance was well correlated with bacterial abundance ($r_S = 0.64$, $p < 0.0001$, $n = 428$; Table 4), showing the strongest correlation for transect A ($r_S = 0.75$, $n = 186$) and the weakest for transect C ($r_S = 0.49$, $n = 117$). The distribution of bacterial abundance showed indeed a similar variation with depth as did viral abundance (Fig. 5). Both viral and bacterial abundances in the upper 200 m (in order to include all stations for statistical analysis) were significantly dependent of the depth and the location of the station in a transect (ANOVA, $p < 0.0001$). We observed VBRs in the upper 200 m as low as 5 and as high as 75. The average VBR (all depths included) was 21 ± 11, independent of the transect or location of the stations (ANOVA, $p > 0.1$). The VBRs at depth >200 m were between 5 and 140, with an average of 26 ± 23.

Viral abundance correlated also with phytoplankton biomass, total Chl *a* and cellular carbon of the smaller-sized phytoplankton ($r_S = 0.50$ and 0.59, respectively, $p < 0.0001$, Table 4). Interestingly, the correlation between viruses and phytoplankton biomass was strongest for transect A and weakest for transect C (Table 4). The spatial vertical distribution of the smaller-sized phytoplankton, numerically dominating the phytoplankton community, showed the same pattern (Fig. 6) as for the 30-m horizontal distribution (Fig. 3C), with the highest abundances in the upper 100 m at stations C1–C6. The algal abundances depended on depth and the transect (ANOVA, $p < 0.0001$) but not of the spatial distribution of the station along the transect ($p = 0.5$). Algal biomass (expressed as carbon or Chl *a*) was, however, also dependent on the distance of the station in a transect (ANOVA, $p < 0.0001$). The depth distribution of the phytoplankton biomass clearly showed a subsurface maximum between 100 and 150 m at stations A3 and A4, which was well below the depth of the euphotic zone (Figs. 7 and 8). Although this distribution corresponded roughly to that of the viral abundance (Fig. 4), it has to be said that the bacteria, as the most abundant potential host of viruses, also showed a significant correlation with algal biomass ($p < 0.0001$, independent of transect; Table 4). First-order partial correlation analysis (freeware http://faculty.vassar.edu/lowry/par.html) indicated that the correlation between phytoplankton biomass and viruses, while controlling for the third inter-correlated variable bacteria, was significant and only partially explained by the correlation between bacteria and phytoplankton. Transect-specific partial correlation analysis showed that transect C was an outlyer, with the correlation between phytoplankton and viruses spuriously caused by the correlation between bacteria and phytoplankton and viruses with bacteria. The bacterial abundance showed specifically for

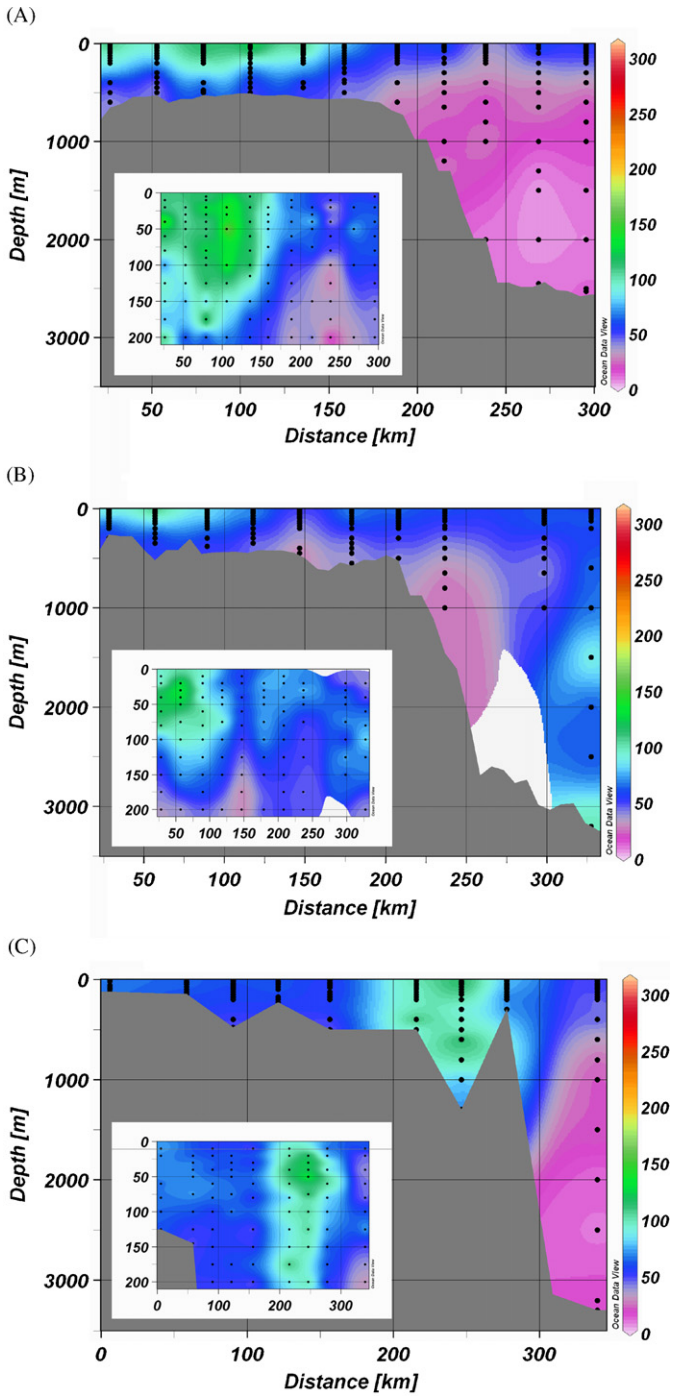

Fig. 4. Depth distribution of the viral abundance ($\times 10^5$ mL^{-1}) during the KEOPS 2005 cruise: (A) transect A, (B) transect B, and (C) transect C. Detailed distribution (0–200 m depth) is shown as inset.

transect C, a strong positive correlation with the smaller-sized phytoplankton abundance ($r_S = 0.83$; Table 4), but not for transects A and B ($r_S = 0.09$ and 0.46, respectively).

4. Discussion

The present study provides a detailed study of virioplankton dynamics in a natural iron-fertilized region southeast of the Kerguelen Islands in the Southern Ocean.

Table 4
Correlations between the viral abundance (virus), the bacterial abundance (bact), and the abundance (algae) and biomass (algal C) of the phytoplankton with cell diameters <20 μm (enumerated by flow cytometry) at transects A, B, and C, using the non-parametric Spearman rank order test

	bact	Chl *a*	algae	algal C
Transect A–C				
Virus	0.642	0.496	0.025	0.587
	0.000	0.000	0.690	0.000
	428	194	194	252
Bact	0.745	0.427	0.473	
	0.000	0.000	0.000	
	198	260	258	
Transect A				
Virus	0.746	0.678	−0.100	0.597
	0.000	0.000	0.318	0.000
	186	83	102	100
Bact	0.769	0.091	0.551	
	0.000	0.359	0.000	
	83	103	99	
Transect B				
Virus	0.609	0.339	0.308	0.717
	0.000	0.043	0.008	0.000
	125	52	74	74
Bact	0.763	0.461	0.419	
	0.000	0.000	0.000	
	42	76	76	
Transect C				
Virus	0.490	0.272	0.224	0.260
	0.000	0.034	0.049	0.022
	117	59	78	78
Bact	0.880	0.826	0.662	
	0.000	0.000	0.000	
	60	81	81	

Presented in vertical order: the Spearman correlation coefficient (r_S), the *p*-value, and the number of samples.

It demonstrates that viral abundance and viral diversity differed between the zone high in Chl *a* (water above the Kerguelen Plateau) and the HNLC waters. Natural iron enrichment induced a zone high in Chl *a* (above the Kerguelen Plateau) that seemed to have a strong structuring effect on bacterioplankton and subsequently on the virioplankton. Also the viral community structure differed between these contrasting regions. Although putative algal virus genomes were detected, virally induced mortality of the smaller-sized (<10 μm) phytoplankton was generally low. Microzooplankton grazing, on the contrary, dominated as loss factor with a profound effect on the regeneration of Fe (see also Obernosterer et al., 2008; Sarthou et al., 2008).

4.1. Viral dynamics

The viral abundance compared well to those reported by Guixa-Boixereu et al. (2002), studying a coastal region

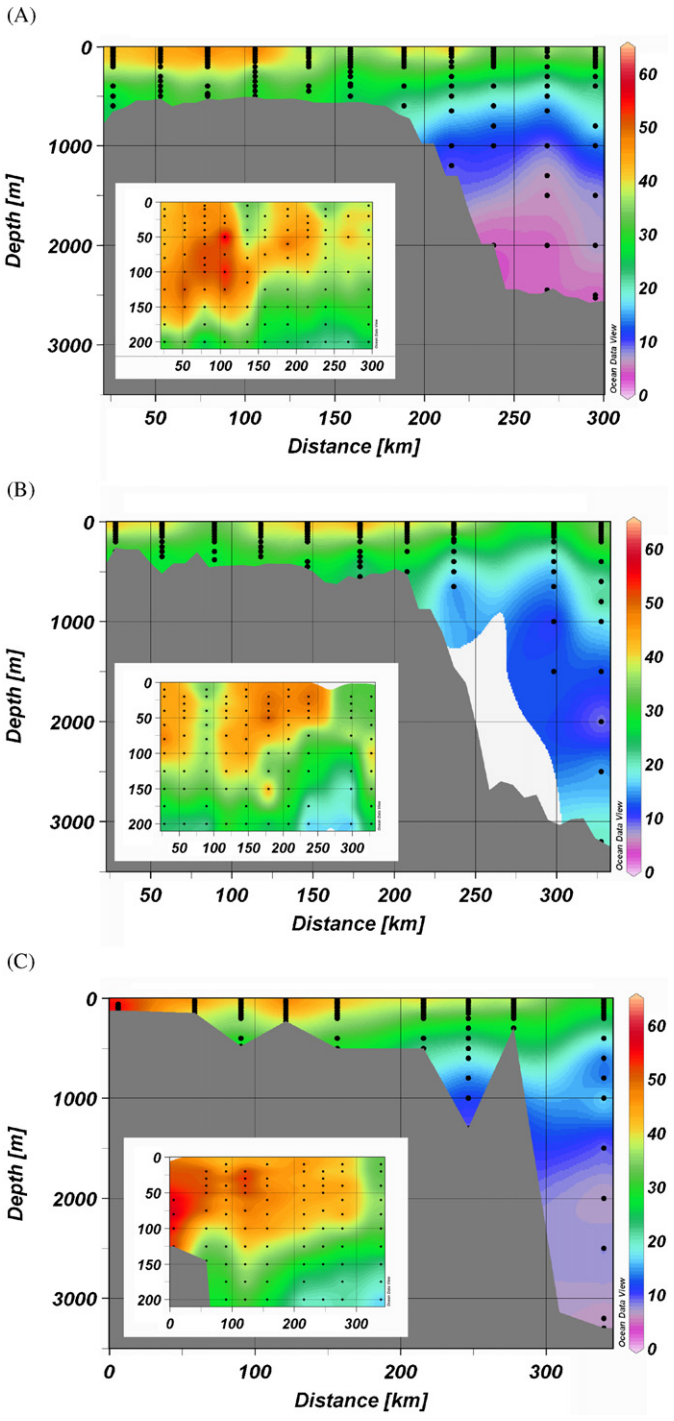

Fig. 5. Depth distribution of the bacterial abundance ($\times 10^4$ mL^{-1}) during the KEOPS 2005 cruise: (A) transect A, (B) transect B, and (C) transect C. Detailed distribution (0–200 m depth) is shown as inset.

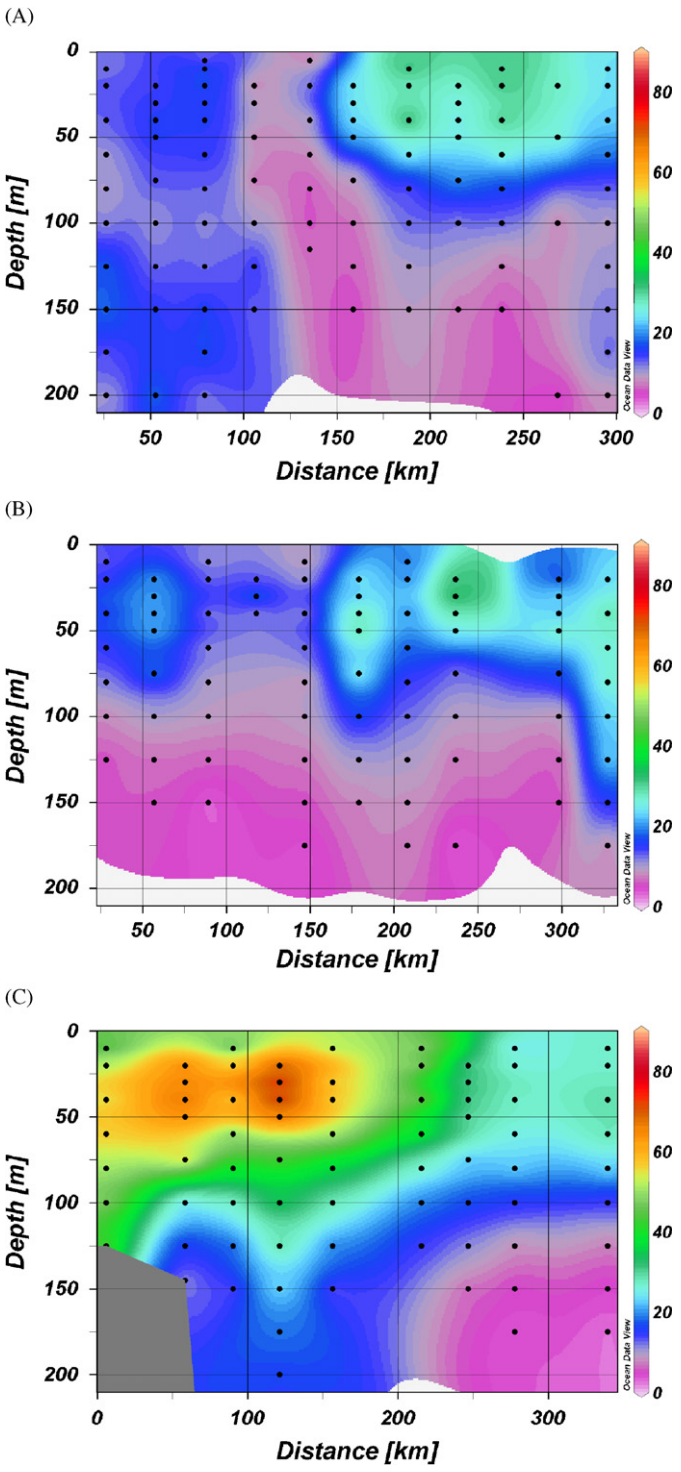

Fig. 6. Depth distribution of the abundance of the phytoplankton with a cell diameter $<20\,\mu$m ($\times 10^2$ mL^{-1}) during the KEOPS 2005 cruise: (A) transect A, (B) transect B, and (C) transect C.

close to the Antarctic Peninsula during the austral summer. Typically, viral abundance increases with the productivity of the system, higher in coastal environments than in open ocean waters (Weinbauer, 2004). In this respect, the majority of stations studied in the KEOPS study site show elevated productivity and should be considered non-typical for the surrounding HNLC waters. The prolonged natural iron fertilization and the consequently elevated productivity and higher biomass over the Kerguelen Plateau (Blain et al., 2007; Lefèvre et al., 2008; Timmermans et al., 2008) resulted in relatively high viral abundance ($1–10 \times 10^6$ mL^{-1}). The viral abundance was up to three-fold higher than in the Southern Ocean between Tasmania and Antarctica

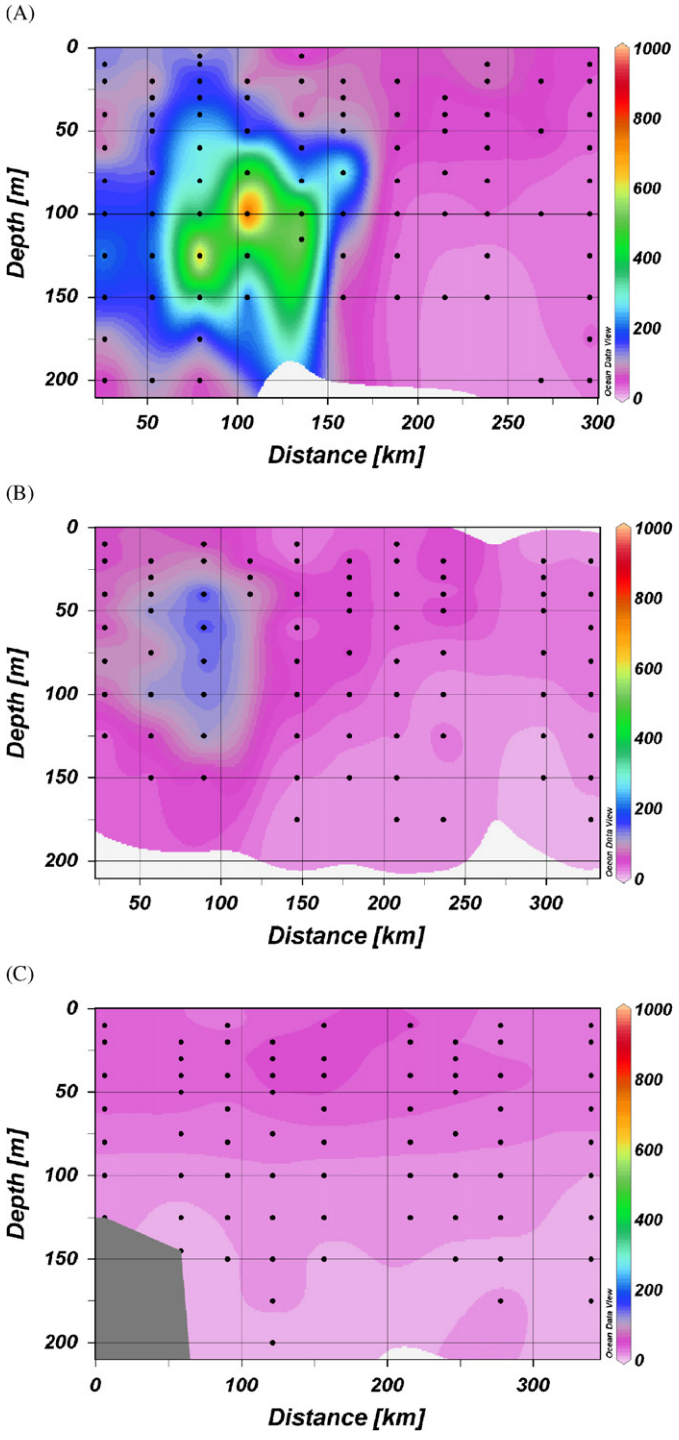

Fig. 7. Depth distribution of the $<20\,\mu m$ phytoplankton biomass ($\mu g\,C\,L^{-1}$) during the KEOPS 2005 cruise: (A) transect A, (B) transect B, and (C) transect C.

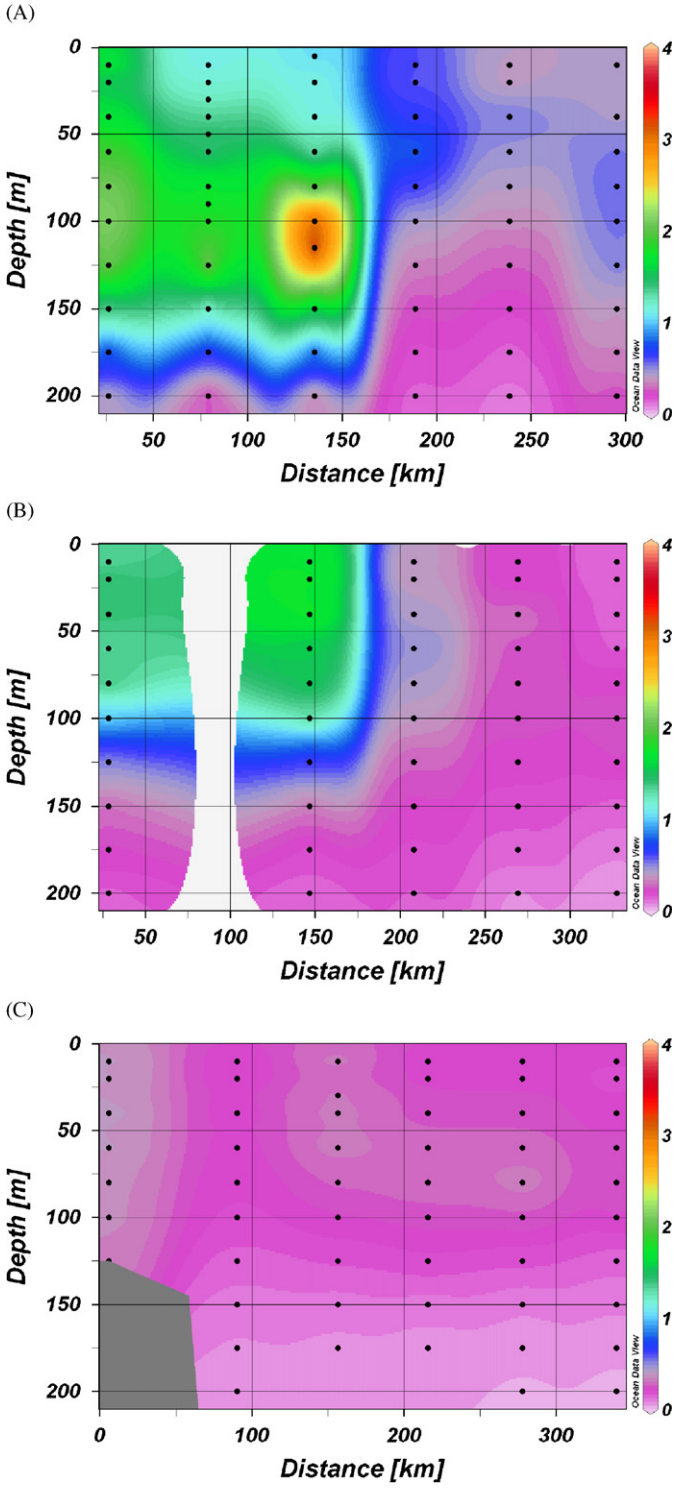

Fig. 8. Depth distribution of the total Chl *a* concentration ($\mu g\,L^{-1}$) during the KEOPS 2005 cruise: (A) transect A, (B) transect B, and (C) transect C.

during spring (Marchant et al., 2000) and in the Drake Passage during the austral summer (Smith et al., 1992).

The general patterns in the vertical distribution of viruses and the numerically dominant bacterial hosts were consistent, with higher abundances in the mixed layer (0–80 m, Mosseri et al., 2008) than in the deeper waters. Both viral and bacterial dynamics depended on depth, but not on transect. Viruses correlated positively with bacteria taking all data into account ($r_S = 0.64$), but the correlation weakened substantially leaving out the deeper waters from the analysis (down to $r_S = 0.2$). The factors affecting production and loss of virus and bacterial host show apparently highest variation in

shallower and more productive waters. The correlation coefficient was comparable to those obtained by others for Antarctic waters in austral summer (Smith et al., 1992; Guixa-Boixereu et al., 2002). Correlations were poor during the austral spring and winter (Smith et al., 1992; Marchant et al., 2000). It seems there is a relationship with time of the year and therefore with the (primary) productivity of the ecosystem. We found that both the viral and bacterial distribution were significantly affected by the location of the stations in a transect, also reflecting the degree of system productivity.

The bacterial abundance was significantly correlated to the phytoplankton biomass, which most likely reflected the response in bacterial community to dissolved organic carbon released by the phytoplankton. This is consistent with the current view that the bacterioplankton in the Southern Ocean are carbon-limited and that the bacterial growth is constrained primarily by the availability of phytoplankton-derived organic matter and not directly by iron (Church et al., 2000; Obernosterer et al., 2008). Ultimately though, this trophic cascade is controlled by the constant supply of iron stimulating phytoplankton productivity. The close coupling between bacterioplankton and phytoplankton was most likely an important underlying factor for the positive correlation between viruses and phytoplankton for transect C.

The VBR was on average about 20, which is higher compared to the typical 5–10 for marine pelagic waters (Weinbauer, 2004) and the 3–15 found in the Southern Ocean (Marchant et al., 2000). The latter study, however, has most likely underestimated virus numbers due to storage loss, which would have reduced the VBR (Wen et al., 2004). Our VBRs are comparable to those reported for the coastal region close to the Antarctic Peninsula (VBR of 18–60, Guixa-Boixereu et al., 2002), and the Drake Passage (VBR of 2–35, Smith et al., 1992). The VBRs were higher for the more productive parts of the study area, which suggests that biological parameters controlling production and loss of bacterial hosts and viruses strongly influenced VBR and virus–bacterium correlations (Wommack and Colwell, 2000). The VBRs in our study were largely determined by variations in viral distribution. The small variation in spatial bacterial distribution seems due to a high mortality of bacteria in the KEOPS study area (Christaki et al., 2008). These authors found that the bacterial production varied five-fold more than bacterial abundance, implying a close coupling between bacterial production and bacterial mortality. In agreement with an earlier study in Antarctic waters by Guixa-Boixereu et al. (2002), bacterivory by heterotrophic nanoflagellates presented the highest impact in the HNLC region (grazing 83–95% of the bacterial production at station C11) and viral lysis in the bloom-dominated region (seven-fold higher viral production rates at station A3 than at C11; Malits, personal communication).

4.2. Viral community structure

The virus community structure showed differences related to depth and to system productivity. The viral group V1, characterized by the lowest green fluorescence after staining with a nucleic acid-specific dye, increased in share with depth. This group is typically considered to consist largely of bacteriophages that can be derived from their relatively small genome size. However, it has to be noted that there is not always a clear relationship between genome size and staining intensity using a nucleic acid-specific dye (Brussaard et al., 2000). Subgroup V2 is also considered to represent mainly different populations of bacteriophages and its distribution was concentrated above the Kerguelen Plateau. This may reflect the elevated production of heterotrophic bacteria in the more productive regions of the study area.

The lower-sized viral genomes did dominate the viral community, with the major peaks occurring at 34 and 68 kb. Similar findings have been reported for surface waters from different locations by Steward et al. (2000). These authors, furthermore, reported that >90% of the virus genomes were to be found in the 26–69 kb range, with at least half between 28 and 45 kb. Our study confirmed these results for transects A and B but not for transect C. At the C-stations, the majority of the viral genomes were between 54 and 75 kb. It may be that these differences are reflected in the bacterial community structure between the transects, but this information is not available. However, other studies including the response of bacterial community composition to iron additions in HNLC waters showed that iron-mediated changes in bacterial communities were remarkably minor (Hutchins et al., 2001; Arrieta et al., 2004).

The viral group V3 with the highest nucleic acid-specific fluorescence may theoretically contain cyanophages and algal viruses (Brussaard et al., 2000). The share of V3 was highest at the more shallow stations, and was interestingly found to be almost two-fold higher for transect C than transect A. Although the smaller-sized phytoplankton biomass at transect A was clearly higher than at transect C, the highest abundance was recorded for transect C (up to three-fold higher). This may have enhanced the contact rate between virus and algal host cell, resulting in successful viral infection and subsequently lysis of the hosts and release of progeny algal viruses (Murray and Jackson, 1992). Highest virally induced rates were indeed recorded at transect C. The viral diversity data were intended to provide quantitative information of the importance of the larger-sized viral genomes for the different transects. The band intensities were, unfortunately, too low to determine their actual contribution. Large-sized viral genomes (95–226 kb), however, were, recorded and the size distribution differed for station A3 and two C-stations. Interestingly, we were able to isolate an algal virus infecting the picophytoplankter *Micromonas pusilla* from surface water originating from

station C11 but were unsuccessful to do so from water from A3.

4.3. Phytoplankton mortality

The use of the serial dilution assay to determine the microzooplankton grazing impact on phytoplankton in iron-limited ecosystems is not new, but to our knowledge, the use of this assay to estimate viral-mediated phytoplankton mortality is. The low standing stock of the algal subpopulations set hurdles to the efficiency of the dilution assay for phytoplankton in the Southern Ocean, but still can yield significant results. Maximum virally induced lysis rate and its respective standard error was $0.18 \pm 0.08\,d^{-1}$ at the HNLC station C11, comparable to microzooplankton grazing of that phytoplankton population ($0.15 \pm 0.05\,d^{-1}$). Overall, however, viral lysis rates appeared not as important as microzooplankton grazing.

The microzooplankton grazing rates compared well to the few other grazer-dilution experiments performed in ecosystems characterized by iron-limitation (Landry et al., 1997; Strzepek et al., 2005). Microzooplankton grazing was an important loss factor, keeping the smaller-sized phytoplankton standing stock at a stable low level (net growth rates varied generally between -0.2 and $0.2\,d^{-1}$). Grazing pressure was, however, selective for the different phytoplankton populations.

Highest growth rates and F_v/F_m values were recorded for transects A and B, illustrative of an algal community that was relieved from iron limitation (Behrenfeld and Kolber, 1999). Microzooplankton grazing rates for the small-sized phytoplankton in this naturally iron-enriched productive region could be as high as $0.62 \pm 0.14\,d^{-1}$ and exceptionally even $1.78 \pm 0.14\,d^{-1}$. The latter was recorded during the first visit of process station A3, taken as a reference for the diatom-dominated algal bloom (Blain et al., 2007). Grazing by microzooplankton exceeded the growth rate of their prey and 45% of the standing stock was eaten daily, clearly demonstrating the relative significance of microzooplankton grazing for the smaller-sized phytoplankton, and contributing to the rather low numerical abundance of the smaller size phytoplankton in the surface waters. After 2 weeks, the growth rate of this 3-μm phytoplankton population had declined by a factor 2 (from 0.42 to $0.24\,d^{-1}$). The concentration of silicic acid was low and the bloom had reached an advanced stage (Mosseri et al., 2008). Concurrently, grazing on this algal groups declined also strongly to only $0.11\,d^{-1}$. Although this matched only 2% of the standing stock, microzooplankton grazing was still responsible for the removal of about half the daily production by this algal group.

4.4. Iron recycling

Our results imply that microzooplankton grazing played a significant role in the regeneration of iron with little or no contribution of virally mediated lysis of phytoplankton. It is new production that is determined by the rate of Fe input but it is the efficiency of iron recycling that determines the system's total production. The biogenic Fe budget of the KEOPS cruise indicates that about half of the total biogenic Fe demand is supplied by Fe input and half by Fe regeneration (Blain et al., 2007; Sarthou et al., 2008). Grazing as well as viral lysis are believed to play a major role in the regeneration of iron (Hutchins and Bruland, 1994; Landry et al., 1997; Poorvin et al., 2004; Strzepek et al., 2005), although viral lysis seems more important for bacterioplankton (Guixa-Boixereu et al., 2002) and grazing for phytoplankton (Bowie et al., 2001; Sarthou et al., 2008; present study).

It is thought that not only the type of prey, but also the mode of regeneration (viral lysis versus grazing) may greatly affect the speciation of released iron and subsequently its bio-availability (Kirchman, 1996; Mioni et al., 2005; Strzepek et al., 2005). Whereas viral lysis releases Fe in an organically complexed form, grazing would result in mainly inorganic Fe (Hutchins and Bruland, 1994; Barbeau et al., 1996; Gobler et al., 1997; Poorvin et al., 2004). We found that the microzooplankton grazing on smaller-sized phytoplankton was more important than viral lysis. Viral lysis did seem an important cause of regeneration of Fe for the heterotrophic bacteria, but the biomass of these numerically dominant organisms was still about eight-fold lower than that of the smaller-sized phytoplankton (10 versus $80\,\mu g\,C\,L^{-1}$). Microzooplankton grazing-mediated regeneration of Fe from phytoplankton seems, thus, to be an essential spoke in the microbial ferrous wheel. Assuming a typical Fe:C (μmol:mol) ratio for the <10-μm phytoplankton of 5 (Bowie et al., 2001; Strzepek et al., 2005; Sarthou et al., 2008), an average uptake rate of $1.9\,pM\,d^{-1}$ was calculated to sustain this phytoplankton community. Furthermore, assuming a 60% regeneration of intracellular Fe by microzooplankton grazing (Landry et al., 1997; Bowie et al., 2001; Sarthou et al., 2008), we estimated an average regeneration rate of Fe of $1.1\,pM\,d^{-1}$. These values compared very well with the values in the biogenic Fe budget of KEOPS station A3 by Sarthou et al. (2008) that were obtained in a completely different manner. These authors showed that microzooplankton at KEOPS station A3 was responsible for the majority of the regenerated Fe and covered 28–48% of the total daily biogenic Fe demand. Our study revealed that a substantial part of this was due to grazing on the <10-μm phytoplankton. Microzooplankton was thus, indeed, found to be relevant player in the regeneration of Fe in both the natural iron-enriched area as well as the HNLC region of the KEOPS study area.

Acknowledgments

We are grateful to the co-ordinator of the KEOPS project S. Blain (Aix-Marseille Université; CNRS) for the opportunity to participate in the cruise. We acknowledge the captain and crew of the R.V. *Marion Dufresne II*, as

well as many of the scientific participants. We are obliged to Harry Witte for helping with the statistical analyses, and we thank Anne-Claire Baudoux for her assistance. This research was financially supported by the Netherlands AntArctic Program (NAAP).

References

Armand, L.K., Quéguiner, B., Mosseri, J., Barthaux, V., 2008. Summer phytoplankton response on the Kerguelen Plateau during the KEOPS program: biomass and diversity. Deep-Sea Research II, this issue [doi:10.1016/j.dsr2.2007.12.034].

Arrieta, J.M., Weinbauer, M.G., Lute, C., Herndl, G.J., 2004. Response of bacterioplankton to iron fertilization in the Southern Ocean. Limnology and Oceanography 49 (3), 799–808.

Barbeau, K., Moffett, J.W., Caron, D.A., Croot, P.L., Erdner, D.L., 1996. Role of protozoan grazing in relieving iron limitation of phytoplankton. Nature 380, 61–64.

Baudoux, A.-C., Noordeloos, A.A.M., Veldhuis, M.J.W., Brussaard, C.P.D., 2006. Virally induced mortality of *Phaeocystis globosa* during a spring bloom in temperate coastal waters. Aquatic Microbial Ecology 44 (3), 207–217.

Behrenfeld, M.J., Kolber, Z.S., 1999. Widespread iron limitation of phytoplankton in the South Pacific Ocean. Science 283, 840–843.

Blain, S., Tréguer, P., Belviso, S., Bucciarielli, E., Denis, M., Desabre, S., Fiala, M., Martin Jézéquel, V., Le Fèvre, J., Mayzaud, P., Marty, J.-C., Razouls, S., 2001. A biogeochemical study of he island mass effect in the context of the iron hypothesis: Kerguelen Islands, Southern Ocean. Deep-Sea Research I 48, 163–187.

Blain, S., Quéguiner, B., Armand, L., Belviso, S., Bombled, B., Bopp, L., Bowie, A., Brunet, C., Brussaard, C., Carlotti, F., Christaki, U., Corbière, A., Durand, I., Ebersbach, F., Fuda, J.-L., Garcia, N., Gerringa, L., Griffiths, B., Guigue, C., Guillerm, C., Jacquet, S., Jeandel, C., Laan, P., Lefèvre, D., Lomonaco, C., Malits, A., Julie, M., Obernosterer, I., Park, Y.-H., Picheral, M., Pondaven, P., Remenyi, T., Sandroni, V., Sarthou, G., Savoye, N., Scouarnec, L., Souhaut, M., Thuiller, D., Timmermans, K., Trull, T., Uitz, J., van-Beek, P., veldhuis, M., Vincent, D., Viollier, E., Vong, L., Wagener, T., 2007. Impacts of natural iron fertilisation on the Southern Ocean. Nature 446, 1070–1075.

Blain, S., Sarthou, G., Laan, P., 2008. Distribution of dissolved iron during the natural iron fertilisation experiment KEOPS (Kerguelen Island, Southern Ocean). Deep-Sea Research II, this issue [doi:10.1016/j.dsr2.2007.12.034].

Bowie, A.R., Maldonado, M.T., Frew, R.D., Croot, P.L., Achterberg, E.P., Fauzi, R., Mantoura, C., Worsfold, P.J., Law, C.S., Boyd, P.W., 2001. The fate of added iron during a mesoscale fertilisation experiment in the Southern Ocean. Deep-Sea Research II 48, 2703–2743.

Brussaard, C.P.D., 2004. Optimization of procedures for counting viruses by flow cytometry. Applied Environmental Microbiology 70 (3), 1506–1513.

Brussaard, C.P.D., Marie, D., Bratbak, G., 2000. Flow cytometric detection of viruses. Journal of Virological Methods 85 (1/2), 175–182.

Christaki, U., Obernosterer, I., Van Wambeke, F., Veldhuis, M.J.W., Garcia, N., Catala, P., 2008. Microbial food web structure in a naturally iron fertilized area in the Southern Ocean (Kerguelen Plateau). Deep-Sea Research II, this issue [doi:10.1016/j.dsr2.2007.12.034].

Church, M.J., Hutchins, D.A., Ducklow, H.W., 2000. Limitation of bacterial growth by dissolved organic matter and iron in the Southern Ocean. Applied Environmental Microbiology 66 (2), 455–466.

De Baar, H.J.W., Boyd, P.W., Coale, K.H., Landry, M.R., Tsuda, A., Assmy, P., Bakker, D.C.E., Bozec, Y., Barber, R.T., Brzezinski, M.A., Buesseler, K.O., Boye, M., Croot, P.L., Gervais, F., Gorbunov, M.Y., Harrison, P.J., Hiscock, W.T., Laan, P., Lancelot, C., Law, C.S., Levasseur, M., Marchetti, A., Millero, F.J., Nishioka, J., Nojiri, Y., van Oijen, T., Riebesell, U., Rijkenberg, M.J.A., Saito, H., Takeda, S., Timmermans, K.R., Veldhuis, M.J.W., Waite, A.M., Wong, C.-S., 2005. Synthesis of iron fertilization experiments: from the Iron Age in the Age of Enlightment. Journal of Geophysical Research 110 (C09S16).

Fuhrman, J.A., 1999. Marine viruses and their biogeochemical and ecological effects. Nature 399, 541–548.

Gobler, C.J., Hutchins, D.A., Fisher, N.S., Cosper, E.M., SanudoWilhelmy, S.A., 1997. Release and bioavailability of C, N, P, Se, and Fe following viral lysis of a marine chrysophyte. Limnology and Oceanography 42 (7), 1492–1504.

Guixa-Boixereu, N., Vague, D., Gasol, J.M., Sanchez-Camara, J., Pedrós-Alió, C., 2002. Viral distribution and activity in Antarctic waters. Deep-Sea Research II 49, 827–845.

Hutchins, D.A., Bruland, K.W., 1994. Grazer-mediated regeration and assimilation of Fe, Zn and Mn from planktonic prey. Marine Ecology Progress Series 110, 259–269.

Hutchins, D.A., Campbell, B.J., Cottrell, M.T., Takeda, S., 2001. Response of marine bacterial community composition to iron additions in three iron-limited regimes. Limnology and Oceanography 46 (6), 1535–1545.

Kirchman, D.L., 1996. Microbial ferrous wheel. Nature 383, 303–304.

Landry, M.R., Hassett, R.P., 1982. Estimating the grazing impact of marine micro-zooplankton. Marine Biology 67, 283–288.

Landry, M.R., Barber, R.T., Bidigare, R.R., Chai, F., Coale, K.H., Dam, H.G., Lewis, M.R., Lindley, S.T., McCarthy, J.J., Roman, M.R., Stoecker, D.K., Verity, P.G., White, J.R., 1997. Iron and grazing constraints on primary production in the central equatorial Pacific: an EqPac synthesis. Limnology and Oceanography 42 (3), 405–418.

Lefèvre, D., Guigue, C., Obernosterer, I., 2008. The metabolic balance at two contrasting sites in the Southern Ocean: above the Kerguelen Plateau and in open ocean waters. Deep-Sea Research II, this issue [doi:10.1016/j.dsr2.2007.12.034].

Marchant, H., Davidson, A., Wright, S., Glazebrook, J., 2000. The distribution and abundance of viruses in the Southern Ocean during spring. Antarctic Science 12 (4), 414–417.

Marie, D., Partensky, F., Vaulot, D., Brussaard, C.P., 1999. Enumeration of phytoplankton, bacteria, and viruses in marine samples. In: Robinson, J.P.E.A. (Ed.), Current Protocols in Cytometry, Suppl. 10. Wiley, New York, pp. 11.11.1–11.11.15.

Mioni, C.E., Poorvin, L., Wilhelm, S.W., 2005. Virus and siderophore-mediated transfer of available Fe between heterotrophic bacteria: characterization using an Fe-specific bioreporter. Aquatic Microbial Ecology 41, 233–245.

Mosseri, J., Quéguiner, B., Armand, L., Cornet-Barthau, V., 2008. Impact of iron on silicon utilization by diatoms in the Southern Ocean: a case of the Si/N cycle decoupling in a naturally iron-enriched area. Deep-Sea Research II, this issue [doi:10.1016/j.dsr2.2007.12.034].

Murray, A.G., Jackson, G.A., 1992. Viral dynamics: a model of the effects of size, shape, motion and abundance of single-celled planktonic organisms and other particles. Marine Ecology Progress Series 89, 103–116.

Obernosterer, I., Christaki, U., Lefèvre, D., Catala, P., Van Wambeke, F., Lebaron, P., 2008. Rapid bacterial remineralization of organic carbon produced during a phytoplankton bloom induced by natural iron fertilization in the Southern Ocean. Deep-Sea Research II, this issue [doi:10.1016/j.dsr2.2007.12.034].

Park, Y-H., Fuda, J-L., Durand, I., Naveira Garabato, A.C., 2008a. Internal tides and vertical mixing over the Kerguelen Plateau. Deep-Sea Research II, this issue [doi:10.1016/j.dsr2.2007.12.034].

Park, Y-H., Roquet, F., Durand, I., Fuda, J-L., 2008b. Large scale circulation over and around the Northern Kerguelen Plateau. Deep-Sea Research II, this issue [doi:10.1016/j.dsr2.2007.12.034].

Poorvin, L., Rinta-Kanto, J.M., Hutchins, D.A., Wilhelm, S.W., 2004. Viral release of iron and its bioavailability to marine plankton. Limnology and Oceanography 49 (5), 1734–1741.

Ruardij, P., Veldhuis, M.J.W., Brussaard, C.P.D., 2005. Modeling the bloom dynamics of the polymorphic phytoplankter *Phaeocystis globosa*: impact of grazers and viruses. Harmful Algae 4, 941–963.

Rue, E.L., Bruland, K.W., 1997. The role of organic complexation on ambient iron chemistry in the equatorial Pacific Ocean and the response of a mesoscale iron addition experiment. Limnology and Oceanography 42, 901–910.

Sarthou, G., Vincent, D., Christaki, U., Obernosterer, I., Timmermans, K.R., Brussaard, C.P.D., 2008. The fate of biogenic iron during a phytoplankton bloom induced by natural fertilization: impact of copepod grazing. Deep-Sea Research II, this issue [doi:10.1016/j.dsr2.2007.12.034].

Smetacek, V., Assmy, P., Henjes, J., 2005. The role of grazing in structuring Southern Ocean pelagic ecosystems and biogeochemical cycles. Antarctic Science 16 (4), 541–558.

Smith, D.C., Steward, G.F., Azam, F., Hollibaugh, J.T., 1992. Virus and bacteria abundances in the Drake Passage during January and August 1991. Antarctic Journal (review).

Steward, G.F., Montiel, J.L., Azam, F., 2000. Genome size distributions indicate variability and similarities among marine viral assemblages from diverse environments. Limnology and Oceanography 45 (8), 1697–1706.

Strzepek, R.F., Maldonado, M.T., Higgins, J.L., Hall, J., Safi, K., Wilhelm, S.W., Boyd, P.W., 2005. Spinning the "ferrous wheel": the importance of the microbial community in an iron budget during the FeCycle experiment. Global Biogeochemical Cycles 19 (GB4S26).

Suttle, C.A., 2005. Viruses in the sea. Nature 437, 356–361.

Timmermans, K.R., Veldhuis, M.J.W., Brussaard, C.P.D., 2008. Probing natural iron fertilization near the Kerguelen (Southern Ocean) using natural phytoplankton assemblages and diatoms cultures. Deep-Sea Research II, this issue [doi:10.1016/j.dsr2.2007.12.034].

Van Heukelem, L., Thomas, C.S., 2001. Computer-assisted high-performance liquid chromatography method development with applications to the isolation and analysis of phytoplankton pigments. Journal of Chromatography A 901, 31–49.

Veldhuis, M.J.W., Timmermans, K.R., 2007. Phytoplankton dynamics during the EISENEX iron fertilisation experiment in the Southern Ocean: a comparative study of field and bottle incubation measurements. Aquatic Microbial Ecology 47, 191–208.

Weinbauer, M.G., 2004. Ecology of prokaryotic viruses. FEMS Microbiology Review. 28, 127–181.

Wen, K., Ortmann, A.C., Suttle, C.A., 2004. Accurate estimation of viral abundance by epifluorescence microscopy. Applied Environmental Microbiology 70 (7), 3862–3867.

Wilhelm, S.W., Suttle, C.A., 1999. Viruses and nutrient cycles in the sea. BioScience 49, 781–788.

Wommack, K.E., Colwell, R.R., 2000. Virioplankton: viruses in aquatic ecosystems. Microbiology and Molecular Biology Reviews 64 (1), 69–114.